EUROFUSION WP15ER-PR(15) 14508

J.M.B. Olsen et al.

Temperature dynamics and velocity scaling laws for warm ion plasma filaments in magnetically confined plasmas

Preprint of Paper to be submitted for publication in
Plasma Physics and Controlled Fusion

This work has been carried out within the framework of the EUROfusion Consortium and has received funding from the Euratom research and training programme 2014-2018 under grant agreement No 633053. The views and opinions expressed herein do not necessarily reflect those of the European Commission.

Temperature dynamics and velocity scaling laws for warm ion plasma filaments in magnetically confined plasmas

Jeppe Olsen

PPFE, Department of Physics, Technical University of Denmark, Building 309, 2800 Kgs. Lyngby

E-mail: jmbols@fysik.dtu.dk

Jens Madsen

PPFE, Department of Physics, Technical University of Denmark, Building 309, 2800 Kgs. Lyngby

E-mail: jmad@fysik.dtu.dk

Anders H. Nielsen

PPFE, Department of Physics, Technical University of Denmark, Building 309, 2800 Kgs. Lyngby

E-mail: ahnie@fysik.dtu.dk

Jens J. Rasmussen

PPFE, Department of Physics, Technical University of Denmark, Building 309, 2800 Kgs. Lyngby

E-mail: jjra@fysik.dtu.dk

Volker Naulin

PPFE, Department of Physics, Technical University of Denmark, Building 309, 2800 Kgs. Lyngby

E-mail: vona@fysik.dtu.dk

Abstract. The influence of electron and ion temperature dynamics on the radial convection of isolated structures in magnetically confined plasmas is investigated by means of numerical simulations. It is demonstrated that the maximum radial velocity of these plasma blobs roughly follows the inertial velocity scaling, which is proportional to the ion acoustic speed times the square root of the filament particle density times the sum of the electron and ion temperature perturbations. Only for small blobs the cross field convection does not follow this scaling. The influence of finite Larmor radius effects on the cross-field blob convection is shown not to depend strongly on the dynamical ion temperature field. The blob dynamics of constant finite and dynamical ion temperature blobs is similar. When the blob size is on the order of 0.1 of the ion

Larmor radius the blobs stay coherent and decelerate slowly compared to larger blobs which dissipate faster due to fragmentation and turbulent mixing.

PACS numbers: 52.30.ex, 52.35.-g, 52.65.-y

Keywords: Velocity scaling, warm ions, scrape-off layer transport, blob dynamics
Submitted to: *Plasma Phys. Control. Fusion*

1. Introduction

It is well established that radial transport of particles and heat out of the confining region of magnetically confined toroidal plasmas and into the region of open magnetic field-lines, known as the scrape-off layer (SOL), is predominantly turbulent [1, 2]. The turbulence in the SOL region is known to be strongly intermittent resulting in broadened particle density and temperature probability distribution functions (PDFs) skewed with a broad tail toward positive perturbations. The intermittent transport is carried in the form of filamentary structures aligned along the magnetic field. The filaments propagate perpendicular to the magnetic field at a significant fraction of the acoustic speed [3–6]. These filamentary structures are known as blobs in low confinement (L-mode) [7–12] and edge localised mode (ELM) filaments in high confinement (H-mode) [13–16]. Although the generation mechanisms for blobs and ELMs are different, the mechanism driving both types of filaments towards the wall is believed to be the interchange drive [13,17–19]. The blobs give rise to problems such as erosion of the main chamber walls where the resulting impurities influence operation parameters such the density disruption limit [19, 20]. The blobs result in peak heat loads at plasma facing components much higher than predicted by classical theory. Predictions of the peak heat loads thus require a thorough understanding of the blob temperature dynamics. In particular, since the ion temperature typically exceeds the electron temperature in a tokamak SOL [21, 22], a proper description requires models which include the temperature dynamics of both electrons and ions. Temperature dynamics is also a necessity for describing the interaction of blobs with neutral particles, e.g. T_e for electron impact ionization and T_i for charge exchange, which, in general, have very strong dependencies on temperature [23]. The blob-neutral interactions define a non-negligible particle source and imply energy and momentum losses and are therefore essential when describing plasma dynamics in a fusion relevant experiment.

Extensive numerical studies of the dynamics of seeded blobs have been made in previous studies [24–27] which have aimed at deducing scaling laws for the radial velocity of blobs. However, most models did not include temperature dynamics and assumed cold ions. Although these simplifications are reasonable in the description of most basic plasma physics experiments [28–30], it is generally not the case in a tokamak SOL.

Recent studies [25, 31–35] have shown that finite ion temperature effects alter the cross field blob transport. Blobs stay coherent and decelerate at a slower rate than cold ion blobs. Furthermore, the observed structures in gas-puff imaging (GPI) observations [36] and finite ion temperature simulations show very similar dynamics. However, the finite ion temperature studies have not included ion temperature dynamics and collisional effects are treated in an ad-hoc manner. Collisional effects influence the cross-field transport blob transport [37] and play an important role in the SOL region profile broadening in the high density limit and in divertor detachment [38]. A consistent model for collisional effects is therefore important for any effort modelling blob transport in the high density limit.

In this paper we investigate the intermittent SOL dynamics including temperature effects in combination with a model with self-consistent perpendicular collisional diffusion. Specifically, we describe the influence of temperature dynamics on the cross-field blob convection and investigate how the radial blob velocity scales with blob size, amplitude, and ion to electron temperature ratio. Furthermore, we investigate the validity of two scaling laws for the maximum radial blob velocity. We use a four-field drift-fluid model, HESEL (Hot Edge-Sol ELectrostatic turbulence), based on the Braginskii equations, describing the evolution of the particle density, generalised vorticity and electron and ion pressure.

The article is outlined as follows: In section 2 we describe the HESEL model used in the simulations. In section 3 we qualitatively describe the effects of including temperature evolution and perturbations on the dynamics of seeded blobs by comparing simulations with different degrees of temperature effects. In section 4 we investigate the effect of different initial parameters on blob dynamics with full temperature evolution and initial perturbations. In section 5 we test the validity of existing blob velocity scalings with different initial parameters. Finally in section 6 we summarise and conclude our results.

2. The HESEL Model

The investigations have been carried out using the HESEL model [39]. HESEL is an energy conserving 2D drift fluid model derived from the Bragiinskii equations using slab geometry, which describes the evolution of four fields: The particle density, n, the generalised vorticity, ω, the electron pressure, p_e, and the ion pressure, p_i. The governing equations are Bohm normalised according to (see for example Ref. [40]),

$$\omega_{ci}t \to t, \quad \frac{\mathbf{x}}{\rho_s} \to \mathbf{x}, \quad \frac{e\phi}{T_{e0}} \to \varphi, \quad \frac{n}{n_0} \to n, \quad \frac{T_e}{T_{e0}} \to T_e, \quad \frac{T_i}{T_{e0}} \to T_i, \tag{1}$$

where $\omega_{ci} = eB_0/m_i$ is the ion cyclotron frequency, $\rho_s = c_s/\omega_{ci}$ is the ion gyroradius at background electron temperature, e is the electron charge, T_{e0} is the background electron temperature, n_0 is the background particle density, B_0 is the magnetic field at major radius R_0, m_i is the ion mass, $c_s = (T_{e0}/m_i)^{1/2}$ is the sound speed and $T_{e(i)}$ is the

electron (ion) temperature. With this normalisation the equations are given as

$$\frac{d}{dt}n + n\mathcal{K}(\varphi) - \mathcal{K}(p_e) = \Lambda_n, \tag{2}$$

$$\frac{d^0}{dt}\omega + \{\nabla\varphi, \nabla p_i\} - \mathcal{K}(p_e + p_i) = \Lambda_\omega, \tag{3}$$

$$\frac{3}{2}\frac{d}{dt}p_e + \frac{5}{2}p_e\mathcal{K}(\varphi) - \frac{5}{2}\mathcal{K}\left(\frac{p_e^2}{n}\right) = \Lambda_{p_e}, \tag{4}$$

$$\frac{3}{2}\frac{d}{dt}p_i + \frac{5}{2}p_i\mathcal{K}(\varphi) + \frac{5}{2}\mathcal{K}\left(\frac{p_i^2}{n}\right) - p_i\mathcal{K}(p_e + p_i) = \Lambda_{p_i}. \tag{5}$$

Here, $d/dt = \partial/\partial t + B^{-1}\{\varphi, \cdot\}$ denotes the convective derivative with the compressible magnetic field, $B(x)\hat{\mathbf{z}} = (B_0R_0)/(R_0 + r_0 + x)\hat{\mathbf{z}}$, where x is the radial position, R_0 and r_0 denote the major and minor radius, respectively, and $\hat{\mathbf{z}}$ is a unit vector parallel to the magnetic field. $d^0/dt = \partial/\partial t + B_0^{-1}\{\varphi, \cdot\}$ denotes the convective derivative with constant magnetic field B_0 and $\mathcal{K}$ is the curvature operator defined as

$$\mathcal{K}(f) = -\frac{\rho_s}{R_0}\frac{\partial}{\partial y}f. \tag{6}$$

The $\mathbf{E}\times\mathbf{B}$ advection is written in the terms of a Poisson bracket defined as

$$\{\varphi, f\} = \frac{\partial\varphi}{\partial x}\frac{\partial f}{\partial y} - \frac{\partial f}{\partial x}\frac{\partial\varphi}{\partial y}. \tag{7}$$

$\omega = \nabla^2(\varphi + p_i)$ is the generalised vorticity, which contains the magnetic field aligned components of the $\mathbf{E}\times\mathbf{B}$ vorticity, $\nabla^2\varphi$, and the ion diamagnetic contribution, $\nabla^2 p_i$. Finite Larmor radius (FLR) effects are thus only included to lowest order, which means that $k_\perp^3\rho_i^3 \ll 1$ is assumed, where $k_\perp$ is the characteristic perpendicular inverse length scale and $\rho_i = (T_{i0}/m_i)^{1/2}\omega_{ci}^{-1}$ is the thermal ion gyroradius (see Ref. [41] and Ref. [31] for a thorough description of FLR effects in drift fluid models). Furthermore we note that the thin-layer approximation is invoked in the vorticity equation (3) assuming small perturbations amplitudes and gradients in the particle density field. HESEL does thus not describe the dynamics of blobs with strong FLR effects or large particle density perturbations accurately.

The terms on the right-hand sides are the dissipative terms and are defined as

$$\Lambda_n = D_n(1+\tau)\nabla^2 n \tag{8}$$

$$\Lambda_\omega = D_i\nabla^2\omega \tag{9}$$

$$\Lambda_{p_e} = D_n\left[\frac{5}{2}(1+\tau)\nabla^2 p_e + \left(\frac{13}{6} - \frac{5}{2}\tau\right)\nabla\cdot(n\nabla T_e) + (1+\tau)\nabla\ln n\cdot\nabla p_i\right] - \frac{3m_e}{m_i}\nu_{ei}(p_e - p_i) \tag{10}$$

$$\Lambda_{p_i} = \left[\frac{5}{2}D_n(1+\tau)\nabla\cdot(T_i\nabla n) - D_n(1+\tau)\nabla\ln n\cdot\nabla p_i + D_i\left(\nabla^2 p_i - p_i\nabla^2\ln n - \nabla\ln n\cdot\nabla p_i\right)\right] + \frac{3m_e}{m_i}\nu_{ei}(p_e - p_i) + p_i\Lambda_\omega, \tag{11}$$

where T_{i0} is the background ion temperature and $\tau = T_{i0}/T_{e0}$. The temperatures are defined as $T_{i,e}(x,y,t) = p_{i,e}(x,y,t)/n(x,y,t)$, both functions of position and time. Note that all parallel effects, including sheath dissipation, have been neglected. The dissipative terms account for friction, electron heat fluxes, and energy exchange due to electron-ion collisions and viscosity and ion heat fluxes due to ion-ion collisions. These collisional terms are written in terms of the diffusion coefficients

$$D_n = (1 + 1.6q^2)\rho_e^2\nu_{ei}, \tag{12}$$

$$D_i = (1 + 1.6q^2)\rho_i^2\nu_{ii}, \tag{13}$$

where ν_{ii} and ν_{ei} are the normalized electron-ion and ion-ion collision frequencies, respectively, $\rho_{i,e} = \omega_{ci,e}^{-1}(T_{i,e0}/m_{i,e})^{1/2}$ are the ion and electron thermal gyroradii and $\omega_{ci,e} = eB_0/m_{i,e}$ are the ion and electron cyclotron frequencies. The diffusion coefficients are evaluated using the background values n_0, T_{e0} and T_{i0}. The $1.6q^2$ factor is the neo-classical Pfirsch-Schlüter correction to the diffusion coefficients, where q denotes the safety factor at the last closed flux surface (LCFS) (see Ref. [42] for a thorough description of these self-consistent diffusive terms).

Previous studies [26,37] have shown that the maximum radial velocity of interchange driven blobs is captured well by the inertial scaling

$$V_{iner} = \gamma\sigma = c_s\left(\frac{\sigma\Delta\Theta}{R\Theta_0}\right)^{1/2}. \tag{14}$$

Here, $\gamma = V/\sigma$ denotes the interchange rate and σ is the characteristic blob size. Θ is an unspecified thermodynamic quantity (e.g. n, p_e, p_i) and Θ_0 is a uniform background. In order to eliminate effects captured by the inertial scaling, we use this normalisation to investigate the differences in blob dynamics.

In order to describe the blob motion, we define the blob centre of mass position

$$\mathbf{x}_{CoM}(t) \equiv \frac{1}{\int(n(x,y,t) - n_0)d\mathbf{x}}\int(n(x,y,t) - n_0)\mathbf{x}d\mathbf{x}, \tag{15}$$

where the integration is over the entire domain and where $\mathbf{x} = (x, y)$ is used to define the position of the blob. To limit the number of free parameters we have chosen to keep the background electron temperature, T_{e0}, the background particle density, n_0, the magnetic field, B_0, the ion mass, m_i and the charge, Z, and the safety factor q fixed throughout the paper. We have chosen parameters typical for ASDEX Upgrade (AUG)

$$T_{e0} = 40 \text{ eV}, \; n_0 = 1 \times 10^{19} \text{ m}^{-3}, \; B_0 = 1.86 \text{ T} \tag{16}$$

$$m_i = 2m_p, \; Z = 1, \; R_0 = 1.65 \text{ m}, \text{ and } r_0 = 0.5 \text{ m}, \tag{17}$$

where m_p is the proton mass.

3. Effect of temperature dynamics

In the following we will describe the effects of including initial temperature profiles and temperature dynamics on the evolution of seeded blobs. The blobs are initialised as

Gaussian perturbations on constant backgrounds

$$n(x,y,0) = n_0 + \Delta n \exp\left(-\frac{(x-x_0)^2+(y-y_0)^2}{2\sigma^2}\right), \tag{18}$$

$$T_e(x,y,0) = T_{e0} + \Delta T_e \exp\left(-\frac{(x-x_0)^2+(y-y_0)^2}{2\sigma^2}\right), \tag{19}$$

$$T_i(x,y,0) = T_{i0} + \Delta T_i \exp\left(-\frac{(x-x_0)^2+(y-y_0)^2}{2\sigma^2}\right), \tag{20}$$

where (x_0, y_0) is the initial blob position, Δn is the initial particle density perturbation amplitude, σ is the initial blob radius, and $\Delta T_{e(i)}$ is the initial electron (ion) temperature perturbation amplitude. The potential, φ, and generalised vorticity, ω, are both initialised to 0. The magnetic field is set to point out of the plane, and the simulations are carried out in a square box with a side length of $L = 40\sigma$. We invoke periodic boundary conditions in the y-direction and apply Dirichlet boundary conditions

$$\phi = 0, \quad \omega = 0, \quad n = n_0, \quad T_e = T_{e0}, \quad T_i = T_{i0} \tag{21}$$

at both radial boundaries $x = 0$ and $x = L_x$. The spatial resolution is $\sigma/dx = 50$ to ensure that the simulations are converged with respect to the size of the simulation domain.

We have investigated the evolution of seeded blobs for four different cases with varying degrees of temperature dynamics included in the governing model equations: 1) Ions are cold except in calculations of the ion diffusion coefficient, D_i, and electron and ion temperature dynamics is neglected. This means that we only solve Eqs. (2)-(3) and neglect all contributions from finite ion temperature effects in the vorticity equation, Eq. (3). 2) Electron temperature dynamics has been included but the ions are cold, which means that we are solving Eqs. (2)-(4), but where the finite ion temperature effects are removed in the same way as in case 1. In case 3) we have included electron temperature dynamics and finite ion temperature effects by setting $p_i(x,y,t) = T_{i0}n(x,y,t)$ at each time step and solving Eqs. (2)-(4). Finally, in case 4) both electron and ion temperature dynamics are included, by solving the full set of HESEL equations, Eqs. (2)-(5). The four cases summarised in Table 1.

Table 1: Detail of temperature dynamics for the four different cases.

Case	Electron temperature	Ion temperature	ΔT_e	ΔT_i
1	$T_{e0} = \text{const.}$	0	0	0
2	$T_e(x,y,t)$	0	$T_{e0}\Delta n/n_0$	0
3	$T_e(x,y,t)$	$T_{i0} = \text{const.}$	$T_{e0}\Delta n/n_0$	0
4	$T_e(x,y,t)$	$T_i(x,y,t)$	$T_{e0}\Delta n/n_0$	$T_{i0}\Delta n/n_0$

In Figure 1 we have plotted the density, vorticity, electron and ion temperatures at $t = 20\gamma^{-1}$ for simulations of all four cases. At $t = 20\gamma^{-1}$ the blobs have moved approximately 5 times their initial size, σ, and differences in the blob convection in the

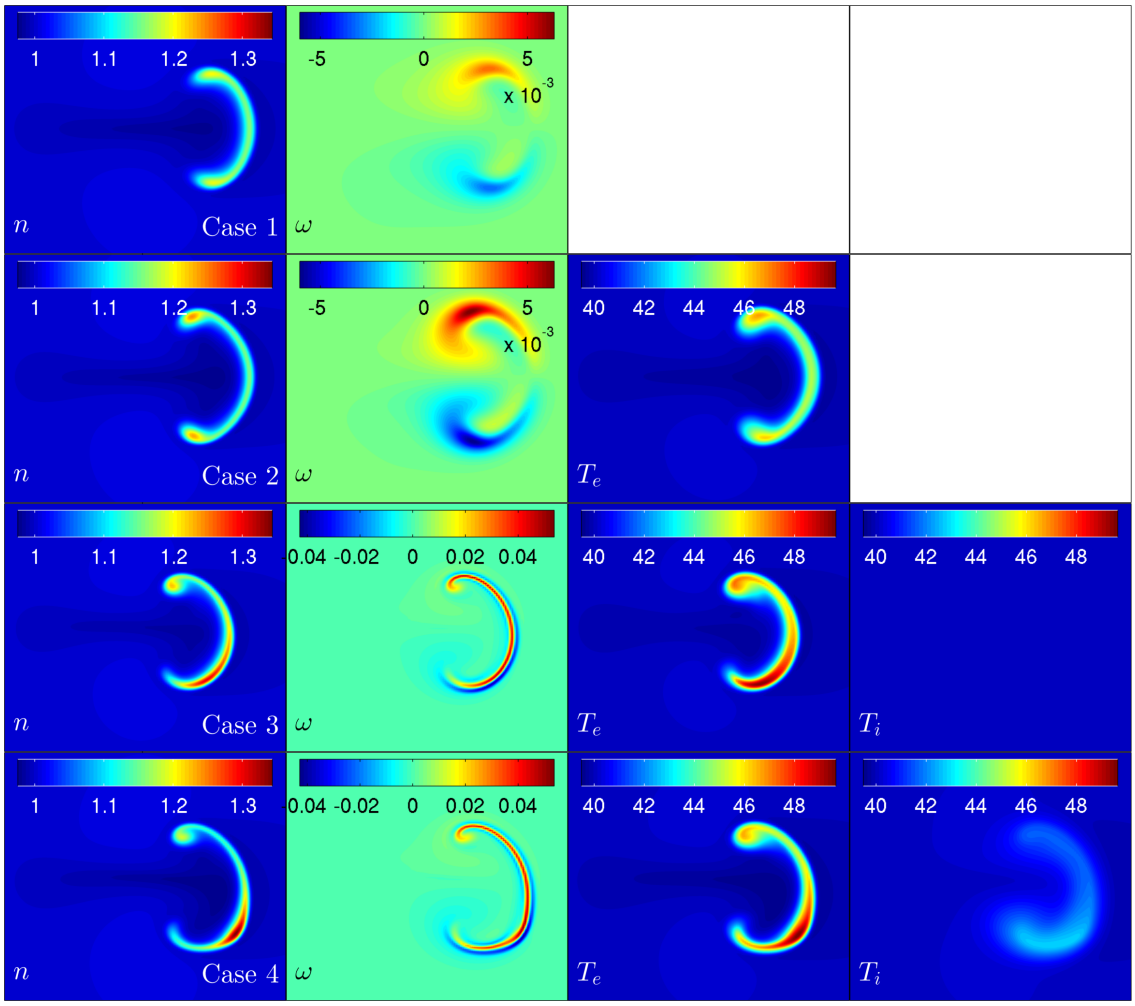

Figure 1: Contour plots of the four fields at $t = 20\gamma^{-1}$. All blobs are initialised with the same parameters, but solved including different degrees of temperature dynamics and perturbations (see Table 1). The boxes only show part of the simulation domain displaying a square box of size $5\sigma \times 5\sigma$.

different simulations are perceptible at this time. For the initial blob size used in this section, $\sigma = 10$, the blobs have moved 5 cm, which is less than the typical SOL region width in AUG. The parameters used for all four simulations are $\Delta n = 0.5n_0$ and $\tau = 1$. Upon comparing case 2 with case 1, we see that the inclusion of electron temperature dynamics causes the blob to spread out more and the lobes behind the front to curl up, but otherwise no big differences are observed. The electron temperature in case 2 is seen to closely resemble the particle density, but due to stronger diffusion, the electron temperature is less localised. !!!!!!!

Looking at case 3 in the third row in Figure 1, it is seen that the most prominent difference between the cold ion simulations and the inclusion of finite ion temperatures is in the vorticity where the up-down symmetry is broken, and the vorticity is elongated along the blob. As a result we see that the up-down symmetry of the blob particle

density is broken and the blob stays more coherent, as was also observed in previous works (see for example Ref. [31]). As shown in the next section the influence of finite ion temperatures is stronger when the ratio of the ion gyroradius to the blob size increases. The bottom plot shows the blob when both electron and ion temperature dynamics are included solving the full set of HESEL equations (case 4). Here, we observe that the symmetry breaking is more profound than in the constant ion temperature case and the blob propagates further downwards. As for the case with no ion temperature effects and electron temperature dynamics, the blob is more spread out and the roll-up of the lobes is stronger. These effects increase with ion to electron temperature ratio. The ion temperature is observed to be less localised than both the electron temperature and the particle density, but it still closely resembles both. This is due to the much stronger diffusion on the ions compared to the electrons (a factor of 10^2). Overall, however, we do not observe significantly different blob dynamics with the inclusion of a dynamic ion temperature compared to the finite ion temperature case.

4. Velocity dependence on blob size, amplitude, and ion temperature

We now move on to examine the effects of different initial parameters on the dynamics of the blobs. Throughout the rest of the paper, the simulations are carried out using the full HESEL model including both electron and ion temperature dynamics. The blobs are initialised according Eqs. (18)-(20) where we vary the initial blob width, σ, the ion to electron temperature ratio, τ, and the initial blob particle density perturbation, Δn. Figure 2 shows the evolution of four different blobs with different initial parameters which capture the general trends of the simulations. For low values of τ, illustrated in the first row, the blob generates the typical mushroom shape seen in for example Ref. [24]. For the high ion temperature blobs, otherwise with the same parameters (second row in Figure 2), the up-down symmetry is broken due to the increased contribution of the ion pressure in the vorticity equation. The high ion temperature blob seen in row 2 propagates in the $\mathbf{B} \times \nabla B$ direction as was also observed in Ref. [31] leaving behind part of the initial mass and propagating as a smaller more coherent structure. The symmetry breaking is not observed for low amplitude blobs as illustrated in the third row of Figure 2. The blob dissipates fast due to collisional diffusion and generates the typical mushroom shape, also seen for low ion temperatures, due to the smaller contribution of the ion pressure to the generalised vorticity. Finally, comparing rows 2 and 4 in Fig. 2, it is seen that larger blobs leave behind more of the initial mass and the curl-up of the lobes is more profound than for smaller blobs.

The curling up of the lobes is, as described in Ref. [31], a consequence of poloidal gradients in the radial component of the advecting $\mathbf{E} \times \mathbf{B}$ velocity field which peaks at $y = 0$. This means that the blob centre is advected faster than the blob sides, which generates the typical mushroom-like shape. As seen in section 3 the blob centre consists of two layers of oppositely signed vorticity. This creates a shear flow which gives rise to the Kelvin-Helmholtz instability [43] resulting in a curling up of the lobes, seen e.g. in

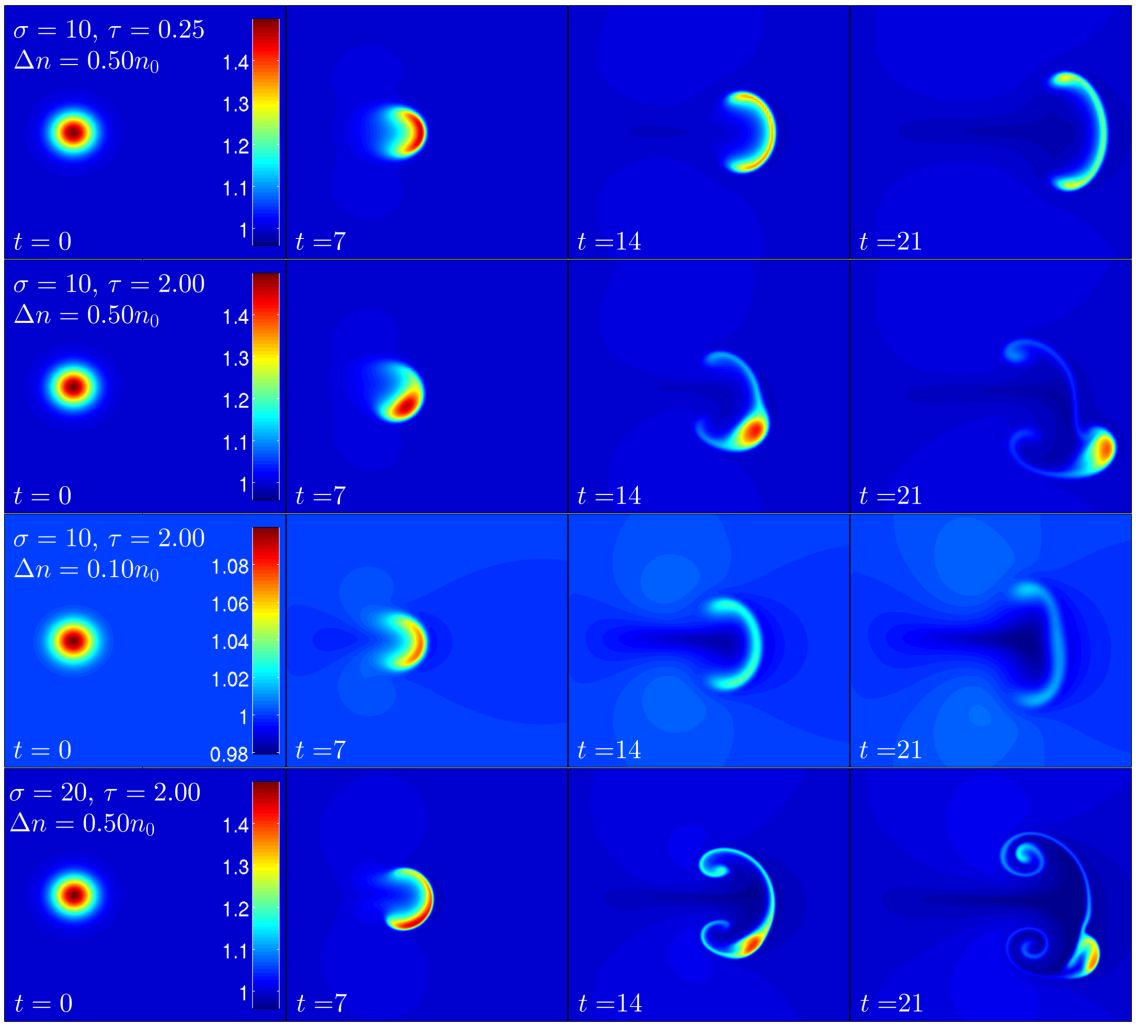

Figure 2: Particle density of four different blobs in time steps of $7\gamma^{-1}$. The displayed domain is a square of size $5\sigma \times 5\sigma$, which is only part of the full simulation domain. The colour scheme is kept constant in each row, and the parameters used in each simulation are stated in the respective rows.

row 4 in Figure 2. The sheared flow is stabilised when FLR effects become significant with increasing $k_\perp \rho_i$. This reduces the curling up of the lobes and causes the blob to stay more coherent [31]. Here, $k_\perp^{-1}$ is the characteristic length-scale which, in the initial phase, is dominated by $k_\perp^{init} \approx \Delta n/\sigma$. This means that low amplitude blobs and large blobs experience weaker FLR effects, as was also observed upon comparing the four cases in Figure 2 where the blobs with stronger FLR effects remained more coherent.

In Figure 3 we have plotted the evolution of the radial centre of mass velocity, $V = d/dt\ x_{com}$, as a function of time for the four cases displayed in Figure 2. We see that all blobs initially accelerate, reach a maximum velocity and then decelerate due to shear flows and collisional diffusion. Upon comparing the black and the blue curve we observe that the velocity of blobs subjected to strong FLR effects flattens at late stages. This flattening can be attributed to the blobs slowing down in the poloidal direction

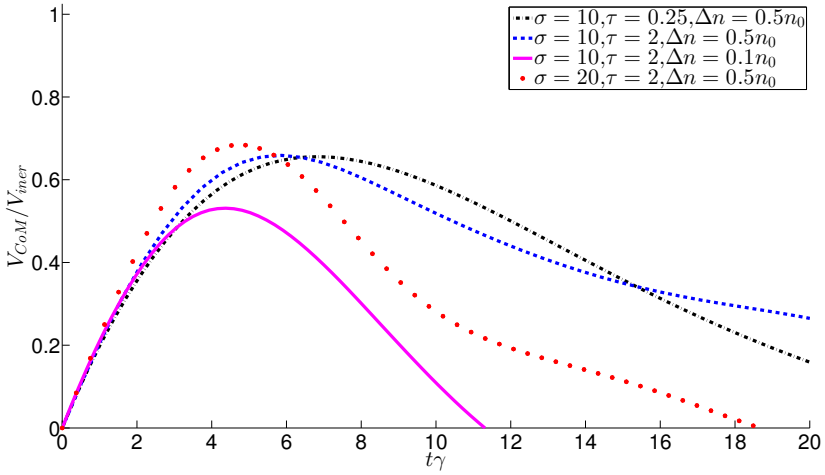

Figure 3: Evolution of the radial centre of mass velocity with time for the four different cases shown in Figure 2.

which leads to a reversal of the poloidal propagation. This reversal in the direction of the poloidal propagation results in a slight radial acceleration seen as the flattening in the blue curve in Figure 3.

The compactness [31], defined as

$$I_c(t) \equiv \frac{\left(\int (n(x,y,t) - n_0) d\mathbf{x}\right) h(x,y,t)}{\left(\int (n(x,y,0) - n_0) d\mathbf{x}\right) h(x,y,0)}, \tag{22}$$

is a measure of blob coherence. Here, h is a Heaviside function given by

$$h(x,y,t) \equiv \begin{cases} 1 & \text{if } (x - x_{max}(t))^2 + (y - y_{max}(t))^2 < \sigma^2 \\ 0 & \text{else,} \end{cases} \tag{23}$$

The integration is over the entire domain, and x_{max}, y_{max} denote the positions of the radial and poloidal maximal particle densities, respectively. I_c thus describes the integrated particle density in a ball of radius σ centred at (x_{max}, y_{max}), normalised to $I_c(t = 0) = 1$. When the particle density is preserved, $I_c = 1$, whereas $I_c \to 0$ for a completely dispersed blob.

In Refs. [31, 32] it was observed that the defining parameter for the blob coherence resulting from FLR effects depends on both initial ion temperature, blob width and blob particle density perturbations. A dimensionless quantity, r, containing these parameters was introduced to quantify the different regimes of the dynamics:

$$r \equiv \frac{\rho_i \Delta n}{\sigma n_0}. \tag{24}$$

The compactness, I_C, at time $t = 10\gamma^{-1}$ is plotted as a function of r in Figure 4. We observe a transition in blob compactness between $r = 0$ and $r = 0.1$, as was also seen in Refs. [31, 32]. By inspection of the simulation results, this is consistent with a transition from plume-like to more coherent structures. The black symbols, which

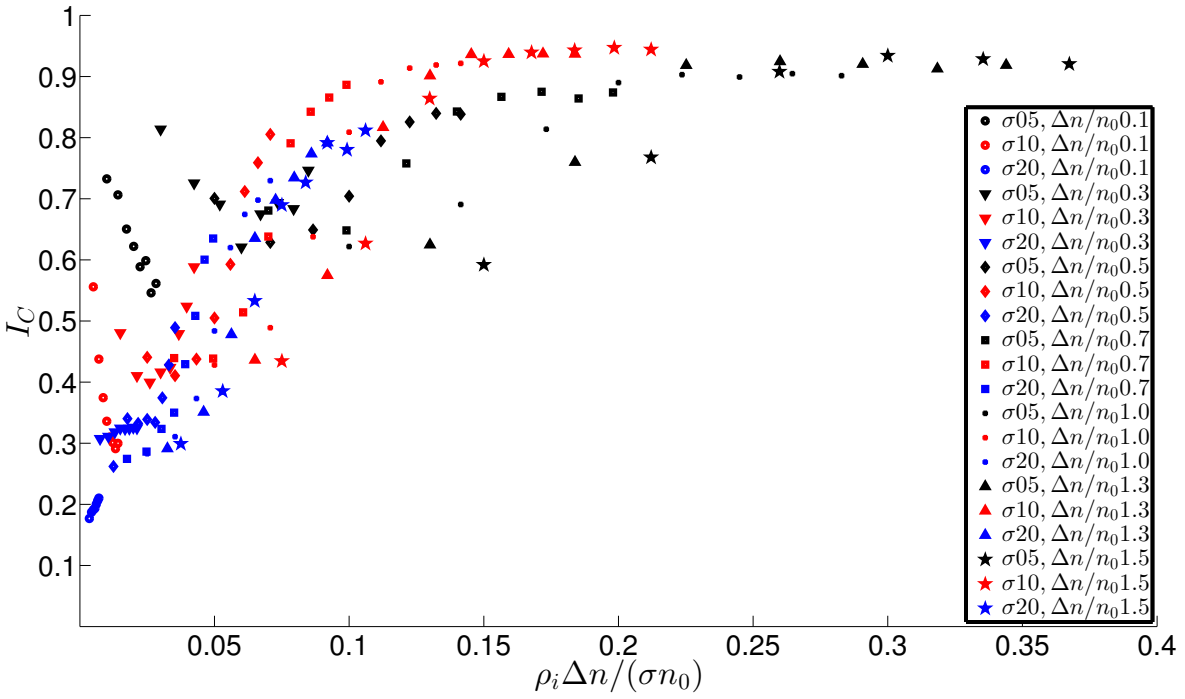

Figure 4: Compactness, I_c, of blobs as a function of $r = \rho_i \Delta n/(\sigma n_0)$ at $t = 10\gamma^{-1}$. A transition from plume-like blobs to more coherent structures between $r = 0$ and $r = 0.1$ is observed.

denote the compactness of small blobs, do not show the same transition as the larger blobs. Instead the small blobs show high compactness for all values of r after 10 γ^{-1}. We believe this is due to a breakdown of the interchange scaling in the extreme cases of very low particle density perturbations and small blob widths, as will be discussed in section 5. At very low Rayleigh number this mismatch of the inertial scaling was also observed by Garcia [5].

5. Velocity scaling laws

We now wish to investigate the validity of two different existing scaling laws for the maximum radial centre of mass velocity, V_{max}. Both scalings are derived based on assumptions similar to what is assumed in the HESEL model i.e. magnetic perturbations and parallel dynamics are neglected. In particular sheath damping is not included. It is therefore reasonable to compare the results from the simulations with the scaling laws.

The first scaling we compare with was introduced in Ref. [26] and is found by balancing the compression of the polarization and diamagnetic currents. It is given by Eq. 14 which, when both ion and electron pressure perturbations are included, is given by

$$1 : \frac{V_{iner}}{c_s} = \left(\frac{\sigma}{R} \frac{(\Delta p_e + \Delta p_i)}{p_0} \right)^{1/2}, \tag{25}$$

where $p_0 = T_{e0} n_0$ is the background electron pressure, and Δp_e and Δp_i are the electron and ion pressure perturbations, respectively. This means that both the particle density perturbation and the electron and ion temperature perturbations contribute to V_{max}, e.g., $\Delta p = n_0 \Delta T + T_0 \Delta n + \Delta n \Delta T$. For all simulations we have initialised the blobs according to Eqs. (18)-(20). With this initialisation, assuming the same form of the electron and ion pressures, Eq. 25 can be rewritten as

$$\frac{V_{iner}}{c_s} = \left(\frac{\sigma}{R} \frac{\Delta p_e}{p_0} \right)^{1/2} (1+\tau)^{1/2}. \tag{26}$$

The second scaling we wish to validate is proposed in Ref. [25] and compared with experimental results in Ref. [44]. It is derived from a model with electron temperature dynamics and finite but constant ion temperature assuming the ion and electron pressure perturbations to be of the same form. This scaling is given by

$$2: \frac{V_{Manz}}{c_s} = \sqrt{\frac{\sqrt{f^2+g^2} - f}{2}}, \tag{27}$$

where

$$f = \left(\frac{\tau \rho_s}{2\sigma} \frac{\Delta p_e}{p_0} \right)^2, \qquad \text{and} \qquad g = (1+\tau) \frac{2\sigma}{R} \frac{\Delta p_e}{p_0}. \tag{28}$$

It is worth noting that in the limit $g \gg f$ Eq. 27 reduces to the inertial scaling, Eq. 26. In the opposite limit, $g \ll f$, the scaling approaches

$$\frac{V_{Manz}}{c_s} \approx \frac{2(1+\tau)\sigma^2}{\tau R \rho_s}. \tag{29}$$

This means that for small blob widths, the limiting behaviour of scaling 2 is proportional to σ^2 and independent of τ and Δp_e.

The validity of these scalings is investigated by calculating V_{max}, normalising it with each scaling and plotting the normalised points. If the scaling fully captures the maximum velocity variation, the points should lie along a horizontal line at $V_{max}/V_{scaling} = 1$ where $V_{scaling}$ is the expected velocity calculated with Eq. (26) or (27). The scalings were, however, not derived to fully describe the velocity, but were derived by simple dimensional analysis and are not the result of e.g. finding a general analytical solution to the full system. The scalings are therefore at most expected to capture the proportionality of V_{max} with the different initial parameters which is the case when $V_{max}/V_{scaling}$ lies along a straight line.

In the following we investigate how V_{max} scales with the initial blob width, amplitude and ion temperature, and test the validity of the proposed scaling laws in Eqs. (26), and (27).

5.1. Dependence on blob width

The first parameter dependence we investigate is the blob width, σ. We display two plots illustrating the general trends in Figure 5, where Figure 5a illustrates V_{max} normalised with c_s and Figure 5b displays V_{max} normalised with V_{iner} (squares) and V_{Manz} (stars).

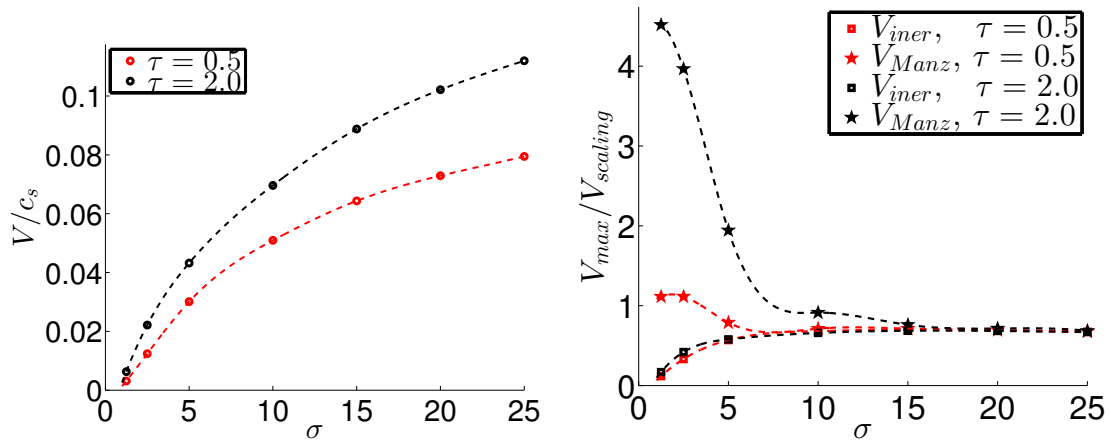

(a) (b)

Figure 5: Maximum blob velocity as a function of initial blob width. The initial particle density perturbation is $\Delta n = 0.5 n_0$. The red symbols are for $\tau = 0.5$ and the black symbols are for $\tau = 2$. The squares are the maximum velocities normalised by scaling 1 and the stars are the maximum velocities normalised by scaling 2.

In the simulation results presented here, the blob amplitude is initialised as $\Delta n = 0.5 n_0$. To illustrate the differences in V_{max} with both weak and strong FLR effects, we have included simulations with two different initial ion temperatures. A case with weak FLR effects, $\tau = 0.5$ (red), and one with stronger FLR effects, $\tau = 2$ (black). It is evident from 5b that neither of the scalings capture the variations in maximum velocity for small blobs $\sigma < 10$. Scaling 1 is found to overestimate the velocity for small blobs, but does however overestimate it in the same way for both weak and strong FLR effects. Scaling 2, on the other hand, displays very different variations in V_{max} for blobs with $\sigma < 10$ with different degrees of FLR effects, where it captures the velocity scaling well for weak FLR effects, but greatly underestimates the velocity for small blobs when FLR effects play a significant role. We note that HESEL assumes that $(\rho_i k_\perp)^3 \ll 1$, which means that it does not capture FLR induced blob dynamics for strong FLR effects correctly. But since scaling 2 is based on assumptions similar to HESEL, this does not explain the observed discrepancies. However, both scalings capture the variations in maximum velocity with blob sizes of $\sigma > 10$ where the points are approximately follow a horizontal line.

5.2. Dependence on ion temperature

Next, we investigate the influence of the initial ion temperature, τ, on V_{max}. Again we display two plots capturing the general trends here illustrated in Figure 6. In both displayed plots the particle density perturbation is set to $\Delta n/n_0 = 0.5$. Figure 6a illustrates V_{max} normalised with c_s and Figure 6b displays V_{max} normalised with V_{iner} (squares) and V_{Manz} (stars). Since the scalings mainly differ for small blobs we examine

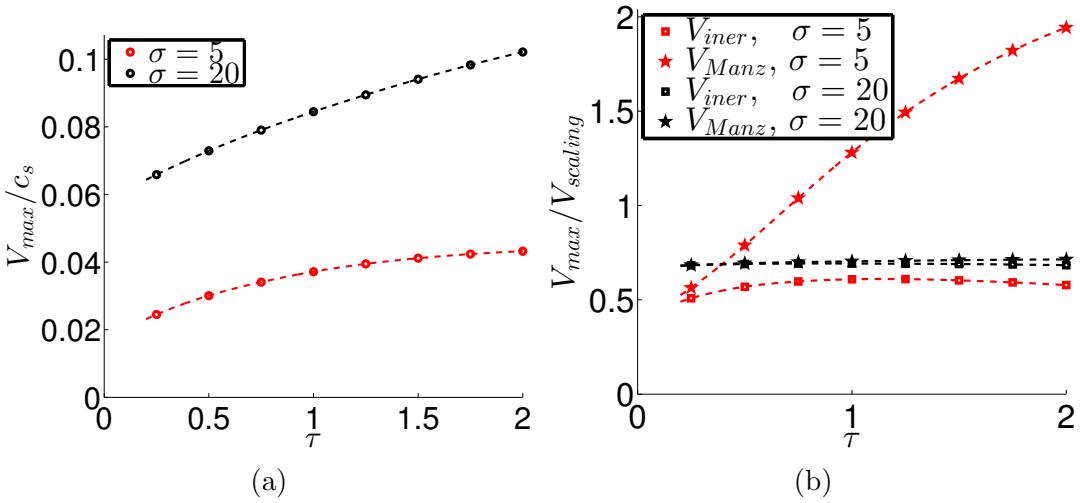

(a) (b)

Figure 6: Maximum blob velocity as a function of initial τ. The initial particle density perturbation is $\Delta n = 0.5 n_0$, the red symbols are for $\sigma = 5$ and the black symbols are for $\sigma = 20$. The squares are the maximum velocities normalised by scaling 1 and the stars are the maximum velocities normalised by scaling 2

how they depend on the initial blob ion temperature for two initial blob widths $\sigma = 5$ and $\sigma = 20$. For both blob sizes, it is seen that scaling 1 (squares) captures the dependence on τ well where the points are very close to being on a straight line for both blob sizes. Scaling 2 also captures the scaling well for large blobs, but does, however, underestimate the velocity dependence on τ for small blobs where it predicts no increase in V_{max} with increasing τ . This is in contrast to what is observed in the HESEL simulations, where the velocity is seen to increase with increasing τ (Figure 6a). This indicates that scaling 2 is partly valid when FLR effects are weak, but does not match when FLR effects are strong.

5.3. Dependence on particle density perturbation

Finally we investigate the influence of the initial blob amplitude, Δn, on V_{max}. In the scalings the dependency on Δn is included in $\Delta p/p_0$. For blobs initialised according to Eqs. (18)-(20) this is proportional to $\Delta n^2 + 2\Delta n$. Again, blobs with a small initial width, $\sigma = 5$, and a large initial width, $\sigma = 20$, are examined. Figure 7 shows the maximum velocity as a function of Δn for blobs with an initial ion temperature of $\tau = 0.5$. For $\Delta n/n_0 < 0.5$ both scalings are observed to overestimate the maximum radial centre of mass velocity. For larger amplitudes $\Delta n/n_0 > 0.5$ scaling 1 describes the maximum velocity variations well where the normalised points approximately follow a horizontal line. Scaling 2, however, underestimates the dependence on Δn for small blobs, as seen in Figure 7b, where the scaling predicts no increase in velocity with Δn. This limiting behaviour is opposite of what is observed in the HESEL simulations, which is displayed in Figure 7a.

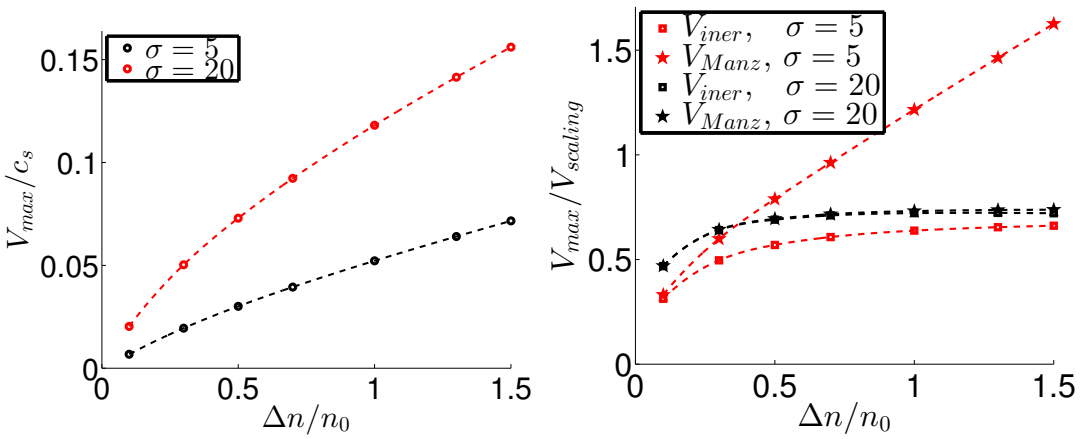

(a) (b)

Figure 7: Maximum blob velocity as a function of initial Δn. The initial ion temperature is $\tau = 0.5$, the red symbols are for $\sigma = 5$ and the black symbols are for $\sigma = 20$. The squares are the maximum velocities normalised by scaling 1 and the stars are the maximum velocities normalised by scaling 2.

6. Conclusion

In this paper we have examined the effects of dynamic temperatures on blob evolution and maximum centre of mass velocity using the HESEL model. We have observed that the inclusion of dynamic ion temperatures do not significantly alter the evolution of the seeded blobs compared to blobs with constant ion temperature. The inclusion of finite ion temperatures does, however, significantly alter the dynamics of the blobs. Finite ion temperatures introduce asymmetries in the blobs due to a contribution of the ion pressure to the vorticity equation. Blobs with zero ion temperature generate the typical mushroom shape, seen in for example [26], whereas the inclusion of finite ion temperatures introduces FLR effects causing blobs to stay more coherent and propagating not only radially, but also poloidally in the ion diamagnetic direction. This transition from mushroom-like structures to coherent filaments can be described by the dimensionless parameter $r = \rho_i \Delta n/(\sigma n_0)$, where a transition is seen between $r = 0$ and $r = 0.1$.

Despite the qualitative differences in the cross-field convection, all blobs initially accelerate radially, reach a maximum velocity and slow down due to stretching and collisional diffusion. We have investigated how this maximum radial velocity scales with different initial parameters, since a scaling estimate of the maximum blob velocities is, e.g., important for estimating power loads. The blob velocity is directly related to the convective density flux carried by the blobs. In this respect we have compared two different scaling laws with the simulation results from HESEL. We have observed that none of the suggested scaling laws cover the whole spectrum of parameters. For blobs larger than $\sigma = 10$ both scaling laws describe the evolution with blob temperature well,

but for blobs with $\sigma < 10$ the scaling given in Eq. (27), denoted as scaling 2, greatly underestimates the velocity, whereas the scaling given in Eq. (26), denoted as scaling 1, slightly overestimates the velocity. The dependence on ion-electron temperature ratio, τ, is observed to be described well by scaling 1 for all parameters, whereas scaling 2 predicts no increase in maximum velocity when strong FLR effects are present, which is opposite of what is observed in the HESEL simulations. For small initial blob particle density perturbations, $\Delta n/n_0 < 0.5$, both scaling laws overestimate the maximum velocity, whereas for large Δn, scaling 1 describes the variations in maximum velocity well. Scaling 2, on the other hand, predicts a constant maximum velocity with increasing particle density perturbation when strong FLR effects are present, which is again not what is observed in the HESEL simulations, where the velocity is seen to increase with increasing particle density perturbations. We have thus concluded that although it does not cover the entire parameter range, scaling 1, which is also the simplest scaling model, is the most successful in describing the maximum radial centre of mass velocity with initial parameters.

We recognise that the present investigation on seeded blobs does not necessarily carry over to self-consistently generated blobs in the turbulence at the edge-SOL region. However, we do believe that once the blobs have been created, they will obey the scalings observed here for seeded blobs. We therefore believe that future investigations in the interaction of blobs with neutrals in the SOL (both impurities and fuelling neutrals) will benefit from the results including temperature dynamics presented here. Both types of neutral interactions are of great interest, where the enhanced ionization by the hot and dense blobs may lead to outward shift of the ionization profiles [45]. This is desired with regard to the impurities resulting from sputtering, which then may not penetrate into the plasma. This is, however, problematic for the fuelling gas which remains in the SOL.

7. Acknowledgements

This work has been carried out within the framework of the EUROfusion Consortium and has received funding from the Euratom research and training programme 2014-2018 under grant agreement No. 633053. The views and opinions expressed herein do not necessarily reflect those of the European Commission.

References

[1] Zweben SJ, Boedo Ja, Grulke O, Hidalgo C, LaBombard B, Maqueda RJ, et al. Edge turbulence measurements in toroidal fusion devices. Plasma Phys. Contr. Fusion. 2007;49(7):S1.

[2] Naulin V. Turbulent transport and the plasma edge. J. Nucl. Mater. . 2007;363-365(1-3):24–31.

[3] Boedo J, Rudakov D, Moyer R, Krasheninnikov S, Whyte D, McKee G, et al. Transport by intermittent convection in the boundary of the DIII-D tokamak. Phys. Plasmas. 2001;8(11):4826–4833.

[4] Antar GY, Counsell G, Yu Y, Labombard B, Devynck P. Universality of intermittent convective

transport in the scrape-off layer of magnetically confined devices. Phys. Plasmas. 2003;10(2) 419-428.

[5] Garcia O, Horacek J, Pitts R, Nielsen A, Fundamenski W, Graves J, et al. Interchange turbulence in the TCV scrape-off layer. Plasma Phys. Contr. Fusion. 2006;48(1):L1.

[6] Grulke O, Terry J, LaBombard B, Zweben S. Radially propagating fluctuation structures in the scrape-off layer of Alcator C-Mod. Phys. Plasmas. 2006;13(1):012306.

[7] Garcia O. Blob transport in the plasma edge: a review. Plasma Fusion Res. . 2009;4:019–019.

[8] Dippolito D, Myra J, Krasheninnikov S. Cross-field blob transport in tokamak scrape-off-layer plasmas. Phys. Plasmas. 2002;9(1):222–233.

[9] D'Ippolito D, Myra J, Krasheninnikov S, Yu G, Pigarov A. Blob Transport in the Tokamak Scrape-off-Layer. Contrib. Plasma Phys. . 2004;44(1-3):205–216.

[10] Krasheninnikov S, D'ippolito D, Myra J. Recent theoretical progress in understanding coherent structures in edge and SOL turbulence. J. Plasma Phys. . 2008;74(05):679–717.

[11] Xu GS, Naulin V, Fundamenski W, Hidalgo C, Alonso JA, Silva C, et al. Blob/hole formation and zonal-flow generation in the edge plasma of the JET tokamak. Nucl. Fusion. 2009;49(9):092002.

[12] Garcia OE, Bian NH, Fundamenski W. Radial interchange motions of plasma filaments. Phys. Plasmas. 2006;13(8):082309.

[13] Fundamenski W, Naulin V, Neukirch T, Garcia OE, Rasmussen JJ. On the relationship between ELM filaments and solar flares. Plasma Phys. Contr. Fusion. 2007;49(5):R43.

[14] Kirk A, Koch B, Scannell R, Wilson H, Counsell G, Dowling J, et al. Evolution of filament structures during edge-localized modes in the MAST tokamak. Phys. Rev. Lett. . 2006;96(18):185001.

[15] Zohm H. Edge localized modes (ELMs). Plasma Phys. Contr. Fusion. 1996;38(2):105.

[16] Kirk A, Wilson H, Counsell G, Akers R, Arends E, Cowley S, et al. Spatial and temporal structure of edge-localized modes. Phys. Rev. Lett. . 2004;92(24):245002.

[17] Rudakov D, Boedo J, Moyer R, Krasheninnikov S, Leonard A, Mahdavi M, et al. Fluctuation-driven transport in the DIII-D boundary. Plasma Phys. Contr. Fusion. 2002;44(6):717.

[18] Gonçalves B, Hidalgo C, Pedrosa M, Silva C, Balbín R, Erents K, et al. Edge localized modes and fluctuations in the JET SOL region. Plasma Phys. Contr. Fusion. 2003;45(9):1627.

[19] Rudakov D, Boedo J, Moyer R, Stangeby PC, Watkins J, Whyte D, et al. Far SOL transport and main wall plasma interaction in DIII-D. Nucl. Fusion. 2005;45(12):1589.

[20] Greenwald M, Terry JL, Wolfe SM, Ejima S, Bell MG, Kaye SM, et al. A new look at density limits in tokamaks. Nucl. Fusion. 1988;28(12):2199.

[21] Kočan M, Gennrich F, Kendl A, Müller H, et al. Ion temperature fluctuations in the ASDEX Upgrade scrape-off layer. Plasma Phys. Contr. Fusion. 2012;54(8):085009.

[22] Kočan M, Gunn J, Pascal JY, Bonhomme G, Devynck P, Ďuran I, et al. Measurements of scrape-off layer ion-to-electron temperature ratio in Tore Supra ohmic plasmas. J. Nucl. Mater. . 2009;390:1074–1077.

[23] Marandet Y, Mekkaoui A, Reiter D, Brner P, Genesio P, Catoire F, et al. Transport of neutral particles in turbulent scrape-off layer plasmas. Nucl. Fusion. 2011;51(8):083035.

[24] Kube R, Garcia OE. Velocity scaling for filament motion in scrape-off layer plasmas. Phys. Plasmas. 2011;18(10):102314.

[25] Manz P, Carralero D, Birkenmeier G, Müller HW, Müller SH, Fuchert G, et al. Filament velocity scaling laws for warm ions. Phys. Plasmas. 2013;20(10):102307.

[26] Garcia O, Bian N, Naulin V, Nielsen A, Rasmussen JJ. Mechanism and scaling for convection of isolated structures in nonuniformly magnetized plasmas. Phys. Plasmas. 2005;12(9):090701.

[27] Yu G, Krasheninnikov S, Guzdar P. Two-dimensional modelling of blob dynamics in tokamak edge plasmas. Phys. Plasmas. 2006;13(4):042508.

[28] Windisch T, Grulke O, Klinger T. Radial propagation of structures in drift wave turbulence. Phys. Plasmas. 2006;13(12):122303.

[29] Furno I, Spolaore M, Theiler C, Vianello N, Cavazzana R, Fasoli A. Direct two-dimensional

measurements of the field-aligned current associated with plasma blobs. Phys. Rev. Lett. . 2011;106(24):245001.

[30] Happel T, Greiner F, Mahdizadeh N, Nold B, Ramisch M, Stroth U. Generation of intermittent turbulent events at the transition from closed to open field lines in a toroidal plasma. Phys. Rev. Lett. . 2009;102(25):255001.

[31] Madsen J, Garcia OE, Stærk Larsen J, Naulin V, Nielsen AH, Rasmussen JJ. The influence of finite Larmor radius effects on the radial interchange motions of plasma filaments. Phys. Plasmas. 2011;18(11):112504.

[32] Wiesenberger M, Madsen J, Kendl A. Radial convection of finite ion temperature, high amplitude plasma blobs. Phys. Plasmas. 2014;21.

[33] Kendl A. Inertial blob-hole symmetry breaking in magnetised plasma filaments. Plasma Phys. Control. Fusion. 2015;57(4):045012.

[34] Jovanović D, Shukla P, Pegoraro F. Effects of the parallel electron dynamics and finite ion temperature on the plasma blob propagation in the scrape-off layer. Phys. Plasmas. 2008;15(11):112305.

[35] Bisai N, Kaw P. Role of ion temperature on scrape-off layer plasma turbulence. Phys. Plasmas. 2013;20(4):042509.

[36] Maqueda RJ, Wurden GA, Stotler DP, Zweben SJ, LaBombard B, Terry JL, et al. Gas puff imaging of edge turbulence (invited). Rev. Sci. Instrum. . 2003;74(3):2020–2026.

[37] Kube R, Garcia OE. Effect of dynamical friction on interchange motion of plasma filaments. Phys. Plasmas. 2012;19(4):042305.

[38] Carralero D, Birkenmeier G, Müller HW, Manz P, deMarne P, Müller SH, et al. An experimental investigation of the high density transition of the scrape-off layer transport in ASDEX Upgrade. Nucl. Fusion. 2014;54(12):123005.

[39] Madsen J. HESEL. To be submitted;

[40] Garcia OE. Two-field transport models for magnetized plasmas. J. Plasma Phys. . 2001;65:81–96.

[41] Scott BD. Nonlinear polarization and dissipative correspondence between low-frequency fluid and gyrofluid equations. Phys. Plasmas. 2007;14(10):102318.

[42] Fundamenski W, Garcia OE, Naulin V, Pitts R, Nielsen AH, Rasmussen JJ, et al. Dissipative processes in interchange driven scrape-off layer turbulence. Nucl. Fusion. 2007;47(5):417.

[43] Bian N, Benkadda S, Paulsen JV, Garcia O. Blobs and front propagation in the scrape-off layer of magnetic confinement devices. Phys. Plasmas. 2003;10(3):671–676.

[44] Manz P, Birkenmeier G, Carralero D, Fuchert G, Müller HW, Müller SH, et al. The influence of finite ion temperature on plasma blob dynamics. Plasma Phys. Control. Fusion. 2015;57(1):014012.

[45] Christensen AS. Interaction with neutrals in SOL toroidal plasmas. Plasma Phys. Control. Fusion (submitted simultaneously with this paper). 2015;